

# Intrinsic Zinc in Brass Enables Lithium Anode Dendrite-Free

Nianchao Zhang<sup>+</sup><sup>[a]</sup>, Jie Wang<sup>+</sup><sup>[b, c]</sup>, Zhiyuan Yang,<sup>[a]</sup> Zheng Zhao,<sup>[b, c]</sup> Congwei Wang,<sup>[b]</sup> Junying Wang,<sup>\*[b, c]</sup> and Junzhong Wang<sup>\*[a]</sup>

Brass foil, composed of copper (Cu) and zinc (Zn), is a commercialized low-cost Cu-based matrix with lithiophilic properties. However, brass has never been employed as a current collector of lithium (Li) metal anode to suppress formation of Li dendrite. Here, we show that brass foil is directly utilized as a current collector for Li metal anodes. It exhibits a stable repeated Li plating and stripping for more than 400 h (200 cycles) with a low overpotential (~0.018 V) and a capacity

of  $1 \text{ mAh cm}^{-2}$  at a current density of  $1 \text{ mA cm}^{-2}$  in a symmetric cell, as well as a higher average Coulombic efficiency of 97.2% for more than 120 cycles with a capacity of  $1 \text{ mAh cm}^{-2}$  at a current density of  $0.5 \text{ mA cm}^{-2}$ . Thanks to the lithiophilicity of homogeneous Zn in brass, the nucleation overpotential of Li is effectively reduced and Li is uniformly deposited on the current collector without dendrite formation. Our investigation might inspire the ancient brass to apply to lithium-ion battery.

## Introduction

Brass foil is an alloy between copper (Cu) and zinc (Zn) where the majority of the elements are copper. Copper foil with lithiophobic properties would induce inhomogeneous lithium (Li) deposition and growth of Li dendrites. Zn with lithiophilic properties can regulate the plating behavior of Li and eliminate the growth of Li dendrite. Mass production of brass is pretty mature. Nevertheless, to our knowledge, the application of brass as Li metal anode current collector has never been reported.

As for Li metal anode, it is considered as a perfect anode for high-energy-density Li metal batteries (Li–S and Li–O<sub>2</sub>)<sup>[1,2]</sup> on account of its high specific capacity ( $3860 \text{ mAh g}^{-1}$ ) and low reduction potential (−3.04 V vs. the standard hydrogen electrode)<sup>[3,4]</sup>. Nevertheless, the practical application of Li metal anode is impeded by several challenges, including the formation of dendritic Li metal during deposition, the crack of solid electrolyte interface (SEI) layer and huge volume change<sup>[5]</sup>. In addition, the uncontrollable and dendrite-forming growth of Li metal will not only induce many “dead Li” with capacity loss

and short cycle life, but also cause potential internal short circuit and safety hazard.<sup>[6,7]</sup>

In recent years, diverse strategies have been proposed in aspects including optimizing electrolyte component,<sup>[8–12]</sup> fabricating solid state electrolyte, constructing artificial SEI/protective layer,<sup>[13–18]</sup> regulating Li<sup>+</sup> distribution with porous interlayer and designing 3D host/composite Li anodes.<sup>[19–26]</sup> To favor Li nucleation, various lithiophilic materials (such as ZnO, TiO<sub>2</sub>, Ag or Au, etc.) have been introduced into 3D hosts.<sup>[27–32]</sup> Very recently, Cui and co-workers creatively demonstrated the selective deposition behavior of Li on different substrate. Li prefers to deposit on the substrate with lower nucleation overpotential (better affinity of Li).<sup>[33]</sup> Materials with zero or low nucleation overpotential can act as nucleation sites for Li deposition and promotes dendrite-free growth of Li. Enlightened by this fabulous work, several current collectors with homogeneous lithiophilic sites are designed and remarkable improvements of electrochemical performance are achieved.<sup>[34–45]</sup> However, to fabricate the lithiophilic current collector, complex procedures and apparatuses are necessary, which restricts large scale production.

Here, we directly use brass foil as a current collector to suppress lithium dendrite formation. We found that Zn homogeneously distributed brass foil with appreciate ratio can direct the deposition morphology of Li, forming a compact and dendrite-free Li metal anode. Symmetric cell with brass foil achieves a stable repeated Li plating and stripping for over 400 h (200 cycles) with a low overpotential (~0.018 V) with a capacity of  $1 \text{ mAh cm}^{-2}$  and at a current density of  $1 \text{ mA cm}^{-2}$  and an elevated average Coulombic efficiency of 97.2% for more than 120 cycles with a capacity of  $1 \text{ mAh cm}^{-2}$  and at a current density of  $0.5 \text{ mA cm}^{-2}$ . We propose the lithiophilic nature of Zn and the uniform distribution of Zn in the Zn–Cu alloy could suppress the formation of Li dendrite on the foil.

[a] Mr. N. Zhang,<sup>+</sup> Mr. Z. Yang, Prof. J. Wang  
Institutes of Physical Science and Information Technology, Anhui Graphene Engineering Laboratory  
Anhui University  
Hefei, Anhui, 230601, China  
E-mail: wangjz@ahu.edu.cn

[b] Dr. J. Wang,<sup>+</sup> Dr. Z. Zhao, A/Prof. C. Wang, A/Prof. J. Wang  
Shanxi Key Laboratory of Carbon Materials, Institute of Coal Chemistry Chinese Academy of Sciences  
Taiyuan 030001, P. R. China  
E-mail: wangjy@sxicc.ac.cn

[c] Dr. J. Wang,<sup>+</sup> Dr. Z. Zhao, A/Prof. J. Wang  
Taiyuan Energy and Material Faculty  
University of Chinese Academy of Sciences  
Taiyuan, P. R. China

[+] These authors contributed equally to this work.

 Supporting information for this article is available on the WWW under  
<https://doi.org/10.1002/batt.202200373>

## Results and Discussion

The Li deposition process and mechanism on brass foil and conventional Cu foil are different, as illustrated in Figure 1. The Li deposition process usually includes two fundamental stages: nucleation and growth. At the start of Li deposition, Li ions are forced to move towards the current collector by electrostatic field and concentration gradient. Once the Li ions get contact with the current collector and obtain electrons, the nucleation is activated. In the case of Cu foil, on account of the surface roughness and lithiophobic nature of Cu, the nucleation sites are scarce and uneven. These unpleasant features not only induce high nucleation overpotential, but also lead to non-uniform Li deposition. In the following growth process, Li tends to deposit on the surface of as deposited Li instead of the lithiophobic Cu surface, generating dendritic structure. Moreover, stronger “tip effect” induced by the dendritic structure further enhances the formation of Li dendrite.<sup>[46]</sup> However, when brass foil was used as the Li anode substrate, the Li deposition process is remarkably improved. Brass is a binary alloy, in which Zn and Cu are homogeneously distributed. According to the Li–Zn phase diagram,<sup>[47]</sup> Zn not only forms alloy with Li, but also shows good solubility in Li. In other words, Zn is lithiophilic and beneficial to pretty low nucleation overpotential when Li deposits on Zn.<sup>[33]</sup> Thus, the homogeneously distributed Zn on the surface of brass can act as lithiophilic nucleation sites during the deposition of Li. Owing to the uniform distribution of nucleation sites, uniform Li deposition is achieved in the initial stage, which favors the subsequently uniform deposition of Li.

The brass foil we employed here is H64 except for special labelling, in which the mass ratio of Cu and Zn is around 64:36 (atomic ratio of Cu/Zn is around 1.81). The only treatment of brass is polish and rinse to guarantee a smooth surface and remove oxides and organic impurities. Figure 3(a) shows the surface morphology of the polished brass, a smooth surface is obtained. As we expected, corresponding Cu (Figure 3b) and Zn (Figure 3c) element mapping images of brass well confirm the homogeneous distribution of Zn and Cu. Since Cu is uniformly distributed and inert to Li, the Cu structure can greatly confines the volume change of Zn during the alloy reaction, which improves the stability of the brass foil

electrode. XRD measurement is conducted to ensure the reaction between Li and Zn. Coin cells with brass foil as working electrode, Li foil as counter/reference electrode are assembled to get lithiated brass foil. After discharge to 0 V, cells are disassembled in a glove box filled with Ar and thoroughly rinsed with DOL (1,3-dioxolane). The XRD patterns of pristine and lithiated brass are summarized in Figure 3(d). The pristine and lithiated brass exhibit three similar reflection peaks around 42°, 49° and 72°, corresponding to (111), (200) and (220) planes of  $\alpha$  phase brass (JCPDS 04-0836), manifesting the good electrochemical stability of brass. Besides, no obvious reflection peaks of LiZn are detected. When the deposition of lithium increased from 2 mAh cm<sup>-2</sup> to 5 mAh cm<sup>-2</sup>, LiOH peak start appearing, but little LiZn was detected yet, as shown in Figure S1. This phenomenon may be induced by the good stability of bulk phase brass and only Zn on the surface of brass foil forms alloy with Li. To confirm the interaction between Li and Zn, more sensitive cyclic voltammogram is employed between 0 and 2 V at a scan rate of 0.1 mV s<sup>-1</sup>. The as assembled cell was first cycled between 0 and 2 V at 50  $\mu$ A for three cycles to exclude the influence of SEI formation on the current density. As shown in Figure 3(e), when brass foil is used as working electrode, drastic increase of cathodic current is observed below 0.2 V, which corresponds to the alloying reaction between Li and Zn.<sup>[48]</sup> However, the voltage profile of Cu foil is very different. No continuous increase of cathodic current appears over the voltage range of 0–0.2 V and the main redox peaks are belonged to oxidation and reduction of Cu.<sup>[16]</sup> What is noteworthy is that the cathodic current is not very high, which indicates only limited Zn reacts with Li. This is in accordance with the XRD measurement.

XPS provides more information on the change of surface elements of the anode in the electrochemical process. As shown in Figure 2, after the deposition of lithium at 0.5 mAh cm<sup>-2</sup> and 5 mAh cm<sup>-2</sup>, the characteristic peaks of Cu 2p and Zn 2p from the brass foil almost disappear while the Li 1s peak is significantly enhanced, which reflect the electrochemical deposition of Li on the surface of brass foil. There is no characteristic peak of LiZn alloy, which is consistent with XRD analysis. The surface morphology of Li deposition appears uniform, as shown in SEM observation (Figure S2).

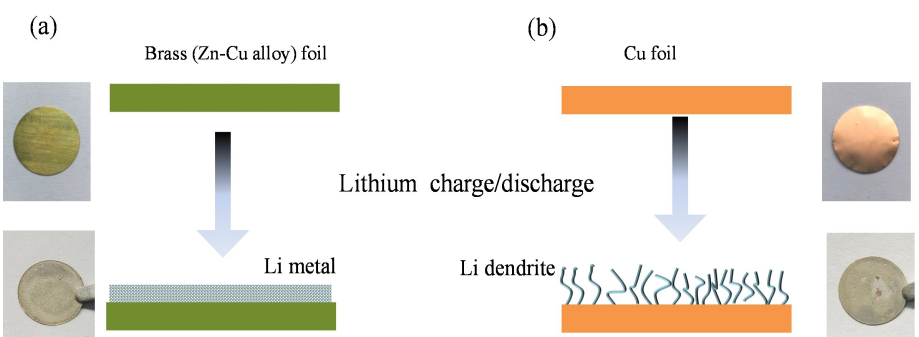


**Figure 1.** Schematic illustrations of Li plating on the a) brass foil electrode and b) Cu foil electrode.

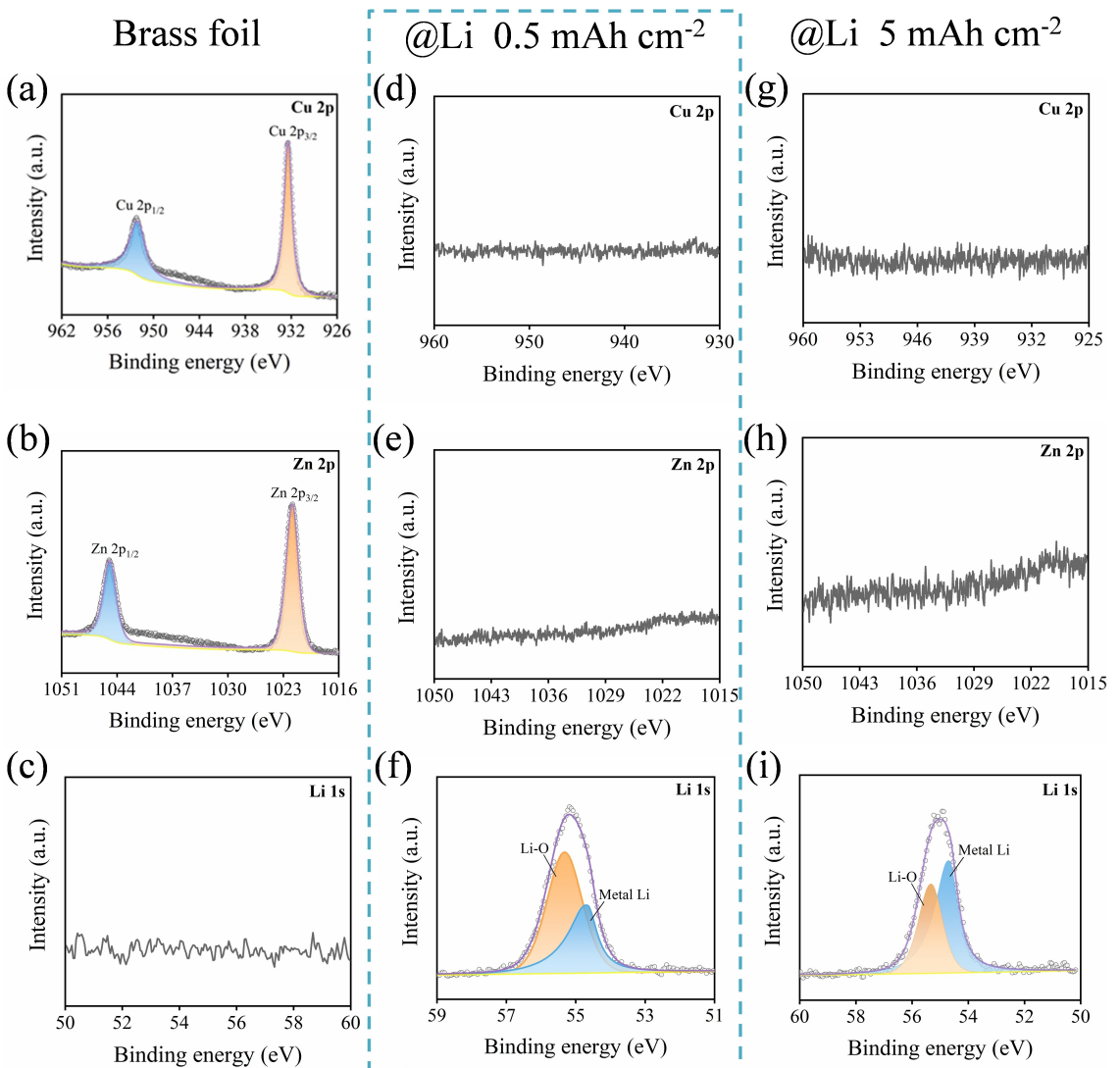


**Figure 2.** High-resolution XPS spectra of brass foil a–c) before and d–i) after deposition of Li at current densities of d–f)  $0.5 \text{ mAh cm}^{-2}$  and g–i)  $5 \text{ mAh cm}^{-2}$ . Cu 2p of a) brass foil, d) brass@Li  $0.5 \text{ mAh cm}^{-2}$  and g) brass@Li  $5 \text{ mAh cm}^{-2}$ . Zn 2p of b) brass foil, e) brass@Li  $0.5 \text{ mAh cm}^{-2}$  and h) brass@Li  $5 \text{ mAh cm}^{-2}$ . Li 1s of c) brass foil, f) brass@Li  $0.5 \text{ mAh cm}^{-2}$  and i) brass@Li  $5 \text{ mAh cm}^{-2}$ .

In addition, the concept of nucleation overpotential is proposed to quantify the degree of lithiophilicity of brass foil and Cu foil. Certain overpotential is a prerequisite to activate and maintain the electrochemical deposition process of Li and is composed of nucleation overpotential and dynamic overpotential. Nucleation overpotential fades away after the activation of the electrochemical deposition, while the dynamic overpotential exists over the electrochemical deposition to overcome the mass-transfer resistance. Specifically, the main factor that influences nucleation overpotential is the lithiophilicity of the electrode surface. The nucleation overpotentials of Li depositing on brass foil and Cu foil are detected by a coin cell configuration with a current density of  $0.3 \text{ mA cm}^{-2}$ . As illustrated in Figure 3(f), a drastic voltage drops of  $0.093 \text{ V}$  (vs.  $\text{Li}/\text{Li}^+$ ) appears at the start of Li deposition when Cu foil is employed as working electrode. After the transitory nucleation stage, the overpotential induced by nucleation gradually

disappears and finally the overpotential is stabilized at  $0.060 \text{ V}$  (vs.  $\text{Li}/\text{Li}^+$ ) by the mass transfer resistance. So, the nucleation overpotential can be calculated as the difference of the initial voltage drop and dynamic overpotential. For Cu foil electrode, the value of nucleation overpotential is about  $0.033 \text{ V}$ . However, the initial voltage drop is only about  $0.066 \text{ V}$ , followed by a stable dynamic overpotential of  $0.059 \text{ V}$ . So, the nucleation overpotential for brass foil electrode is only around  $0.007 \text{ V}$  and much smaller than Cu foil electrode. The sharp nucleation overpotential gap between brass foil electrode and Cu one should origin from the different surface property. Benefiting from the homogeneous distribution and lithiophilicity of Zn, Li prefers to form a compact and smooth morphology, rather than form dendritic structure.

As we expected, Li deposition morphology on the two types of electrodes is well consistent with the distinguishing nucleation overpotentials (Figure 4). Figure 4(a and b) shows

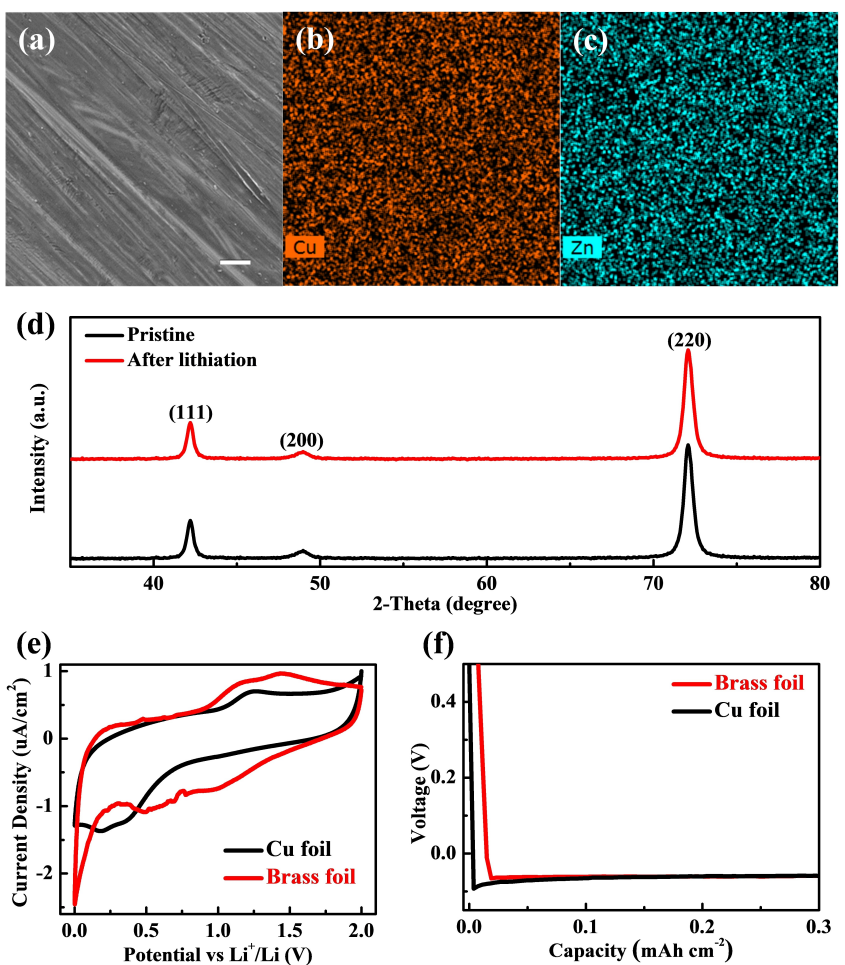


**Figure 3.** SEM image of a) brass foil electrode. Corresponding b) Cu and c) Zn element mapping images of brass foil electrode. d) XRD patterns of pristine brass foil and brass foil after lithiation. e) Comparison of cyclic voltammogram of brass foil electrode and Cu foil electrode with Li counter electrode at a sweep rate of 0.1 mV s<sup>-1</sup>. f) Voltage profiles during initial Li deposition at 0.3 mA cm<sup>-2</sup> onto two types of electrodes. Scale bars in (a–c) 10 μm.

the SEM images of the pristine morphology of brass foil electrode and Cu electrode, and both electrodes possess relatively flat surface. However, with 1 mAh cm<sup>-2</sup> Li deposited (at a current density of 0.5 mA cm<sup>-2</sup>), tremendous morphology difference appears on the two types of electrodes. For brass foil electrode, Li uniformly deposits on the surface of electrode, exhibiting compact and smooth surface without discernable formation of Li dendrite (Figure 4c and e). In contrast, abundant Li dendrites cover the surface of Cu electrode, indicating uneven growth of Li (Figure 4d and f). Moreover, the compact and smooth morphology is still maintains when more Li (2 mAh cm<sup>-2</sup>) is deposited on the brass foil electrode (Figure S2).

To explore the anode usage, coin cells are assembled to investigate the electrochemical performances. First, we tested the long cycling stability of the two types of electrode with symmetrical cells. 4 mAh cm<sup>-2</sup> of Li was predeposited onto the two types of electrodes to forming brass@Li and Cu@Li anodes. Figure 5(a) displays the voltage profiles of brass@Li and Cu@Li symmetrical cells with a capacity of 1 mAh cm<sup>-2</sup> and at a current density of 1 mA cm<sup>-2</sup>. Unexpectedly, brass@Li maintains an extremely low overpotential (~0.018 V) for more than 400 h.

In contrast, Cu@Li exhibits a relatively stable overpotential (~0.029 V) in the initial 100 h and the voltage profile starts to fluctuate randomly in the following cycles. The unstable cycling performance of Cu@Li symmetrical cell may be attributed to unstable Li/electrolyte interface and the electrical disconnection resulting from repetitive growth and dissolution of Li dendrites.<sup>[24]</sup> To show more details of the voltage-time profiles of brass@Li and Cu@Li, 51–70 cycles and 151–170 cycles of the two types of anodes are amplified in Figure 5(c and d). Since the repetitive evolution of Li dendrites causes spatial variation in localized reaction kinetics on the electrode surface, the voltage profile of the Cu@Li symmetrical cell shows large overpotential fluctuation in every depositing and dissolving process. In comparison, smooth and steady voltage profile is well maintained in the brass@Li symmetrical cell during the whole cycles. Moreover, when applying a higher current density (2 mA cm<sup>-2</sup>) to the two types of symmetrical cells, the brass@Li symmetrical cell exhibits a low overpotential (~0.025 V) with no obvious overpotential fluctuation for over 120 h, while the Cu@Li symmetrical cell gets unstable after around 80 h (Figure S3).

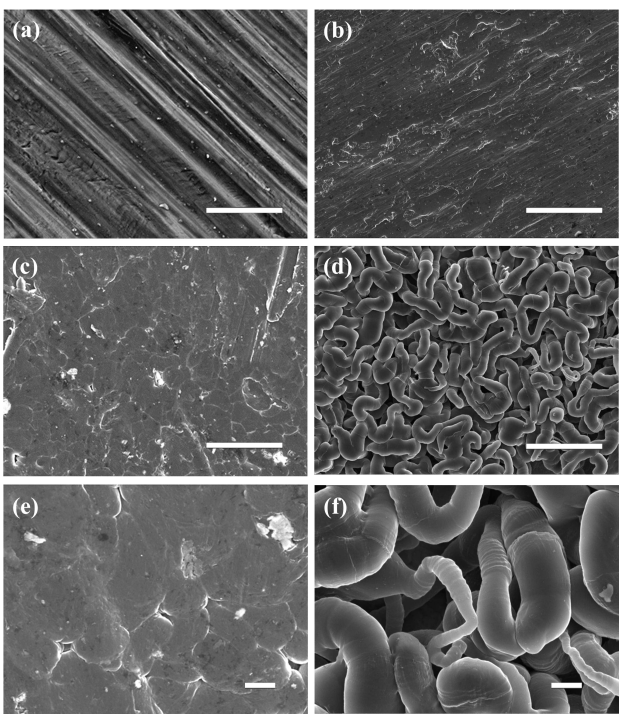


**Figure 4.** The morphology of a) pristine brass foil electrode and b) Cu foil electrode. The morphology of c, e) brass foil electrode and d, f) Cu foil electrode after Li plating with a current density of  $0.5 \text{ mA cm}^{-2}$  and a plating capacity of  $1 \text{ mAh cm}^{-2}$ . Scale bars in (a-d)  $10 \mu\text{m}$  and (e and f)  $1 \mu\text{m}$ .

EIS analysis was conducted on the two types of symmetric cells before cycling and after 10 cycles (Figure 5e and Figure S5) to study the interfacial properties of the two kinds of cells, which further supports the reduced polarization and enhanced cycling stability of cell with brass@Li. The interfacial resistance of SEI and charge transfer resistance on the anode surface can be quantified as the semi-circle in high frequency region of relevant Nyquist plots.<sup>[19]</sup> Before cycling, the interfacial resistance for brass@Li and Cu@Li is 49 and  $71 \Omega$ , respectively (Figure 5e). After cycling with a capacity of  $1 \text{ mAh cm}^{-2}$  and a current density of  $1 \text{ mA cm}^{-2}$  for 10 cycles, the interfacial resistance is 12 and  $17 \Omega$ , respectively (Figure S5). More Li metal deposition after cycling would remove the oxide on the foil surface and reduce the interface resistance. The equivalent circuits are shown in Figure S7. The reduced interfacial charge transfer resistance further indicates that more favorable Li depositing/dissolving dynamics and better electrode stability would be achieved with brass@Li.

Coulombic efficiency is another key index to assess the performance of lithium metal electrode, which is defined as the ratio of the Li dissolution capacity and Li deposition capacity in the same cycle.<sup>[17]</sup>  $1 \text{ mAh cm}^{-2}$  of Li was deposited on the electrode and then stripped away from the electrode until the voltage reaches  $0.5 \text{ V}$  at a current density of  $0.5 \text{ mA cm}^{-2}$ . It can be clearly seen that cells with brass foil present stable electrochemical cycling behavior with high Coulombic efficiency, while cells with Cu foil show poor cycling performance with gradually degressive Coulombic efficiency (Figure 5b). In detail, cells with brass foil and Cu foil both show relatively low initial

Coulombic efficiency ( $\sim 92\%$  for brass foil and  $\sim 93\%$  for Cu foil). The Coulombic efficiency of cell with brass foil steadily increases in the first several cycles and then stabilizes over  $97.5\%$  for 120 cycles. The average Coulombic efficiency is about  $97.2\%$ . For cell with Cu foil, the Coulombic efficiency exhibits the same tendency as that of the brass foil in the first few cycles, but suffers a drastic decline after 50 cycles (only  $88.6\%$  after 80 cycles). The poor Coulombic efficiency of cell with Cu foil reflects the formation of Li dendrite and the loss of active Li. In contrast, the uniform Li deposition guided by brass foil suppresses the loss of active Li and favors a high Coulombic efficiency. Furthermore, when paired with LiFePO<sub>4</sub> cathode, brass@Li also shows better cycling stability than Cu@Li (Figure 5f).

We also investigated the effects of the mass ratio of Zn in the foil on the performances of the Li deposition and full cell with LiFePO<sub>4</sub> cathode. Commercial brass foils with different mass ratio of Cu from 59% to 80% compared to pure Zn were tested, as shown in Figure 6. The samples H65 (Cu65Zn35, atomic ratio of Cu/Zn is 1.87) and H64 (Cu64Zn36) are more stable than other ones (pure Zn, H59 (Cu59Zn41) and H80 (Cu80Zn20) in the Li deposition (Figure 6a) and the full cell (Figure 6b). Those data indicated that the Zn ratio has a significant effect on the performances of foil current collector with the optimization of 35%–36% Zn in copper matrix that is able to supply with good lithiophilicity and uniform Li nucleation sites but avoid Zn–Li alloy formation.

## Conclusion

In summary, we have demonstrated that brass with lithiophilic Zn uniformly distributed in the foil can guide even nucleation and growth of Li and suppresses the formation of Li dendrite. The homogenous nature of brass yields ubiquitous and uniform Zn distribution, which favors the uniform nucleation in the initial stage of Li deposition. The uniform nucleation further promotes dendrite-free Li deposition on brass foil. Brass (around 64% Cu) foil electrode exhibits an impressive electrochemical performance. The Coulombic efficiency of the brass foil electrode with a capacity of  $1 \text{ mAh cm}^{-2}$  and at a current density of  $0.5 \text{ mA cm}^{-2}$  maintains at  $97.2\%$  for over 120 cycles. Moreover, in the test of systematic cell, brass@Li shows remarkably low overpotential and enhanced cycling stability at the current densities of  $1 \text{ mA cm}^{-2}$  and  $2 \text{ mA cm}^{-2}$ . This ancient alloy strategy may shed a light on the design of lithiophilic electrode for safe and high-performance Li metal battery.

## Experimental Section

### Electrode preparation

A piece of brass foil (thickness =  $50 \mu\text{m}$ ) was firstly mechanically polished with abrasive papers to remove oxides and organic impurities on the surface. Then the polished foil was rinsed by deionized water and alcohol for several times. After drying at room

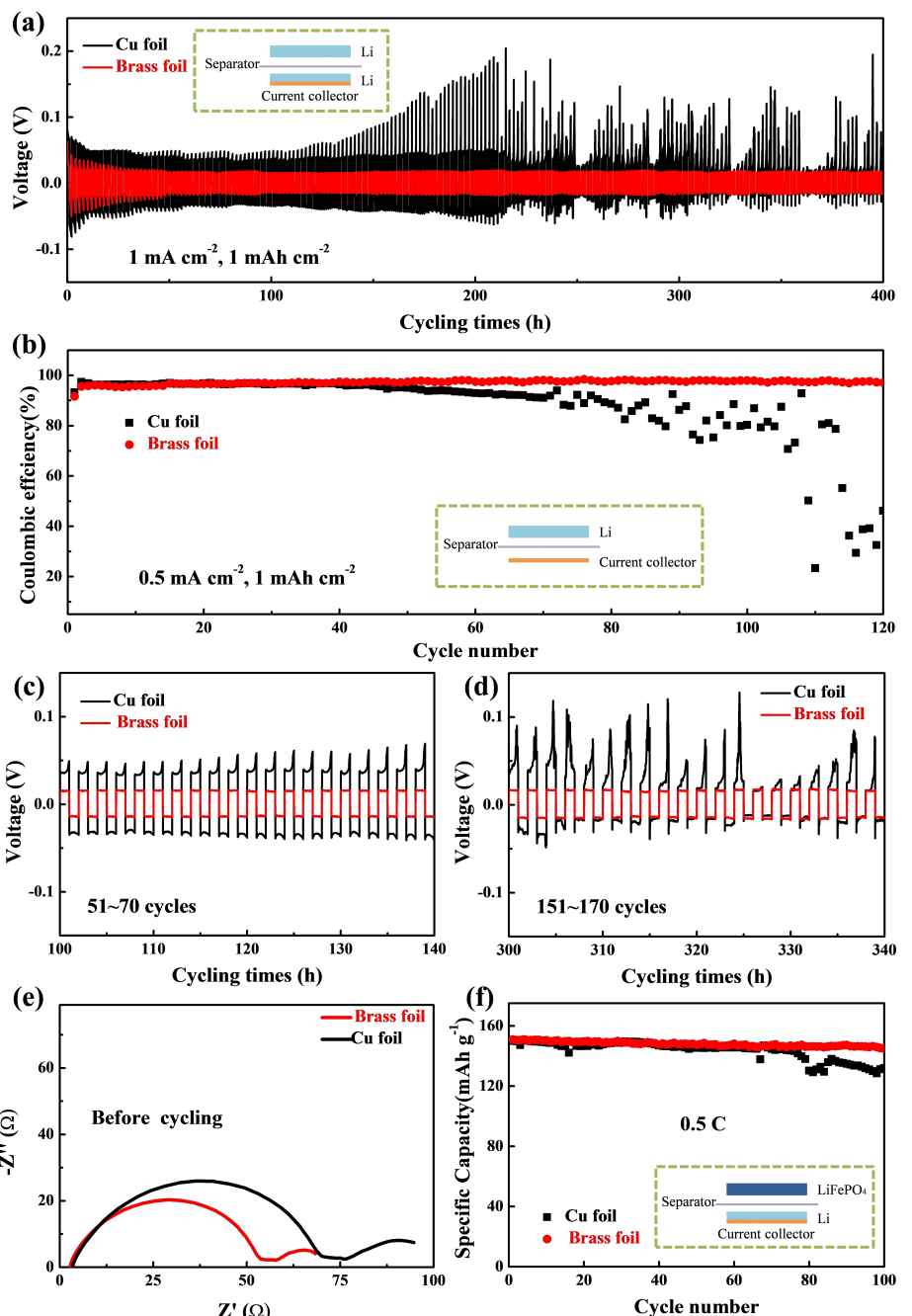


**Figure 5.** a) Voltage-time profiles for symmetric cells with Cu@Li electrode or brass@Li electrode at a current density of  $1 \text{ mA cm}^{-2}$  with a stripping/plating capacity of  $1 \text{ mAh cm}^{-2}$ . b) Comparison of Coulombic efficiency of brass foil electrode and Cu foil electrode at a cycling capacity of  $1 \text{ mAh cm}^{-2}$  and a current density of  $0.5 \text{ mA cm}^{-2}$ . c) The enlarged voltage profiles from the 51<sup>st</sup> to the 70<sup>th</sup> cycle in (a). d) The enlarged voltage profiles from the 151<sup>st</sup> to the 170<sup>th</sup> cycle in (a). e) The Nyquist curves of symmetric cells with Cu@Li electrode or brass@Li electrode before cycling at a current density of  $1 \text{ mA cm}^{-2}$  with a cycling capacity of  $1 \text{ mAh cm}^{-2}$ . f) Cycling performance of full cells for brass@Li anode and Cu@Li anode at  $0.5 \text{ C}$  using LiFePO<sub>4</sub> as the cathode (based on the theoretic capacity of LiFePO<sub>4</sub>).

temperature in vacuum for 6 h, the foil was punched into circular disks ( $\phi 12 \text{ mm}$ ) for further utilization.

### Characterization

XRD patterns were recorded on a RigakuD/MAX 2500/PC diffractometer using Cu K $\alpha$  radiation ( $\lambda = 0.154 \text{ nm}$ ). XPS was carried out on the Thermo ESCALAB 250 spectrometer with an Al-K $\alpha$  X-ray source with a  $500 \mu\text{m}$  electron beam spot. SEM measurements

were conducted on a field emission scanning electron microscope (JSM-7001F) at 5 kV. To characterize the morphology of deposited lithium on brass foil and Cu foil, the cells were carefully disassembled in a glove-box filled with argon to get the lithium-deposited anodes, then the anodes were gently rinsed with DOL (1,3-dioxolane) for three times to remove the residual electrolyte and lithium salts and totally dried in the glove-box at room temperature.

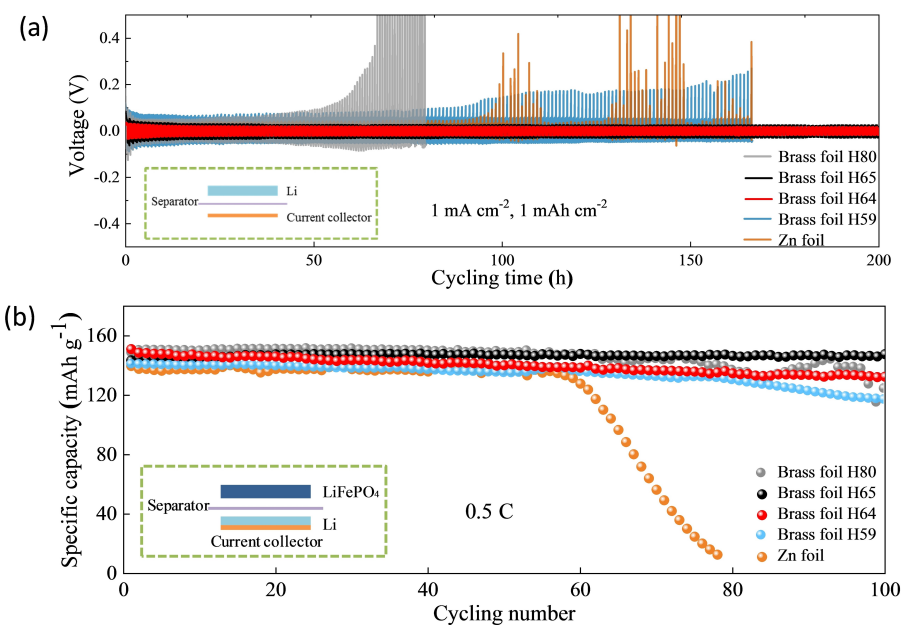


**Figure 6.** a) Voltage-time profiles for symmetric cells with different Zn mass ratio foils at a cycling capacity of  $1 \text{ mAh cm}^{-2}$  and a current density of  $1 \text{ mA cm}^{-2}$ . b) Cycling performance of full cells for various brass@Li anodes and Zn@Li anode at  $0.5 \text{ C}$  using LiFePO<sub>4</sub> as the cathode (based on the theoretic capacity of LiFePO<sub>4</sub>).

## Electrochemical measurements

To evaluate the electrochemical performance, CR2016 coin cells were assembled in a glove-box filled with argon. Brass foil or Cu foil was used as the working electrode, lithium metal foil ( $\phi 12 \text{ mm}$ ) was used as the reference and counter electrode, 1 M LiTFSI in DOL (1,3-dioxolane)/DME (1,2-dimethoxyethane) ( $V/V = 1:1$ ,  $40 \mu\text{L}$ ) with 1.0 wt% LiNO<sub>3</sub> additive was used as the electrolyte and Celgard 2400 membrane was used as the separator. The cells were first cycled between 0 and 0.5 V at  $50 \mu\text{A}$  for five cycles on a LAND battery system to stabilize the SEI. To measure the Coulombic efficiency, a fixed amount of  $1 \text{ mAh cm}^{-2}$  lithium was first deposited on the current collector at a current density of  $0.5 \text{ mA cm}^{-2}$ , then the deposited lithium was stripped away with a cut-off voltage of 0.5 V at the same current density. For the symmetric cell test,  $4 \text{ mAh cm}^{-2}$  of lithium was first deposited on the current collector, and then cycled at a current density of 1 or  $2 \text{ mA cm}^{-2}$  and with a cycling capacity of  $1 \text{ mAh cm}^{-2}$ . For the LiFePO<sub>4</sub> full cells, the LiFePO<sub>4</sub> electrodes were prepared by mixing LiFePO<sub>4</sub>, PVDF (polyvinylidene fluoride), and carbon black in the mass ratio of 8:1:1 with NMP (N-methyl-2-pyrrolidone) as the solvent. The areal mass loading of the LiFePO<sub>4</sub> electrodes was around  $2.7 \text{ mg cm}^{-2}$ . The brass foil electrode or Cu foil electrode was first assembled into a half cell with a lithium metal foil as counter electrode. After plating  $1 \text{ mAh cm}^{-2}$  of lithium metal onto the electrode, the cell was disassembled in an Ar-filled glove box and Cu@Li electrode or brass@Li electrode was further reassembled into a full cell against LiFePO<sub>4</sub> cathode. The electrolyte was the same as that in the half cells. These cells were galvanostatically cycled between 2.5 and 4 V at  $0.5 \text{ C}$ .

Cyclic voltammogram (CV) measurement of the brass foil and Cu foil was performed using a Princeton Applied Research Multi-Channel Potentiostat between the voltage window ranging from 0 to 2 V at a scan rate of  $0.1 \text{ mVs}^{-1}$ . Electrochemical impedance spectroscopy (EIS) was measured at room temperature between 100 kHz and 0.1 Hz with an amplitude of 5 mV after specific cycles.

The EIS was carried out after the symmetrical cells cycled at  $1 \text{ mA cm}^{-2}$  with a cycling capacity of  $1 \text{ mAh cm}^{-2}$  at different cycles.

## Acknowledgements

This work was supported by National Natural Science Foundation of China (22179138), Natural Science Foundation of Shanxi Province (2021030212300) and Shanxi Major Project (20181102026).

## Conflict of Interest

The authors declare no conflict of interest.

## Data Availability Statement

The data that support the findings of this study are available on request from the corresponding author. The data are not publicly available due to privacy or ethical restrictions.

**Keywords:** brass · current collector · lithium metal anode · lithiophilic · symmetric cells · zinc

- [1] P. G. Bruce, S. A. Freunberger, L. J. Hardwick, J.-M. Tarascon, *Nat. Mater.* **2012**, *11*, 19–29.
- [2] X.-B. Cheng, R. Zhang, C.-Z. Zhao, Q. Zhang, *Chem. Rev.* **2017**, *117*, 10403–10473.
- [3] W. Xu, J. Wang, F. Ding, X. Chen, E. Nasybulin, Y. Zhang, J.-G. Zhang, *Energy Environ. Sci.* **2014**, *7*, 513–537.
- [4] D. Lin, Y. Liu, Y. Cui, *Nat. Nanotechnol.* **2017**, *12*, 194.

- [5] Z. Luo, X. Qiu, C. Liu, S. Li, X. Ji, *Nano Energy*. **2021**, *79*, 105507.
- [6] F. Ding, W. Xu, G. L. Graff, J. Zhang, M. L. Sushko, X. Chen, Y. Shao, M. H. Engelhard, Z. Nie, J. Xiao, X. Liu, P. V. Sushko, J. Liu, J.-G. Zhang, *J. Am. Chem. Soc.* **2013**, *135*, 4450–4456.
- [7] X. Liang, Q. Pang, I. R. Kochetkov, M. S. Sempere, H. Huang, X. Sun, L. F. Nazar, *Nat. Energy*. **2017**, *2*, 17119.
- [8] N.-W. Li, Y.-X. Yin, J.-Y. Li, C.-H. Zhang, Y.-G. Guo, *Adv. Sci.* **2016**, *4*, 1600400.
- [9] Y. Lu, Z. Tu, L. A. Archer, *Nat. Mater.* **2014**, *13*, 961.
- [10] W. Li, H. Yao, K. Yan, G. Zheng, Z. Liang, Y.-M. Chiang, Y. Cui, *Nat. Commun.* **2015**, *6*, 7436.
- [11] J. Qian, W. A. Henderson, W. Xu, P. Bhattacharya, M. Engelhard, O. Borodin, J.-G. Zhang, *Nat. Commun.* **2015**, *6*, 6362.
- [12] K. Qin, K. Holguin, M. Mohammadirooudbari, J. Huang, E. Young Sam Kim, R. Hall, C. Luo, *Adv. Funct. Mater.* **2021**, *31*, 2009694.
- [13] C. Heubner, S. Maletti, H. Auer, J. Hüttl, K. Voigt, O. Lohrberg, K. Nikolowski, M. Partsch, A. Michaelis, *Adv. Funct. Mater.* **2021**, *31*, 2106608.
- [14] X.-B. Cheng, T.-Z. Hou, R. Zhang, H.-J. Peng, C.-Z. Zhao, J.-Q. Huang, Q. Zhang, *Adv. Mater.* **2016**, *28*, 2888–2895.
- [15] B. Zhu, Y. Jin, X. Hu, Q. Zheng, S. Zhang, Q. Wang, J. Zhu, *Adv. Mater.* **2016**, *29*, 1603755.
- [16] Y. Liu, D. Lin, Y. Yuen Pak, K. Liu, J. Xie, H. Dauskardt Reinhold, Y. Cui, *Adv. Mater.* **2016**, *29*, 1605531.
- [17] G. Zheng, S. W. Lee, Z. Liang, H.-W. Lee, K. Yan, H. Yao, H. Wang, W. Li, S. Chu, Y. Cui, *Nat. Nanotechnol.* **2014**, *9*, 618.
- [18] W. Liu, P. Liu, D. Mitlin, *Adv. Energy Mater.* **2020**, *10*, 2002297.
- [19] D. Lin, Y. Liu, Z. Liang, H.-W. Lee, J. Sun, H. Wang, K. Yan, J. Xie, Y. Cui, *Nat. Nanotechnol.* **2016**, *11*, 626.
- [20] T.-T. Zuo, X.-W. Wu, C.-P. Yang, Y.-X. Yin, H. Ye, N.-W. Li, Y.-G. Guo, *Adv. Mater.* **2017**, *29*, 1700389.
- [21] R. Zhang, X.-B. Cheng, C.-Z. Zhao, H.-J. Peng, J.-L. Shi, J.-Q. Huang, J. Wang, F. Wei, Q. Zhang, *Adv. Mater.* **2016**, *28*, 2155–2162.
- [22] L. Liu, Y.-X. Yin, J.-Y. Li, N.-W. Li, X.-X. Zeng, H. Ye, Y.-G. Guo, L.-J. Wan, *Joule* **2017**, *1*, 563–575.
- [23] Q. Li, S. Zhu, Y. Lu, *Adv. Funct. Mater.* **2017**, *27*, 1606422.
- [24] Q. Yun, Y.-B. He, W. Lv, Y. Zhao, B. Li, F. Kang, Q.-H. Yang, *Adv. Mater.* **2016**, *28*, 6932–6939.
- [25] L.-L. Lu, J. Ge, J.-N. Yang, S.-M. Chen, H.-B. Yao, F. Zhou, S.-H. Yu, *Nano Lett.* **2016**, *16*, 4431–4437.
- [26] H. Zhao, D. Lei, Y.-B. He, Y. Yuan, Q. Yun, B. Ni, W. Lv, B. Li, Q.-H. Yang, F. Kang, J. Lu, *Adv. Energy Mater.* **2018**, *8*, 1800266.
- [27] M. Liu, X. Guan, H. Liu, X. Ma, Q. Wu, S. Ge, H. Zhang, J. Xu, *Chem. Eng. J.* **2022**, *445*, 136436.
- [28] M. Huang, Z. Yao, Q. Yang, C. Li, *Angew. Chem. Int. Ed.* **2021**, *60*, 14040–14050.
- [29] Q. Wu, Y. Zheng, X. Guan, J. Xu, F. Cao, C. Li, *Adv. Funct. Mater.* **2021**, *31*, 2101034.
- [30] Q. Yang, M. Cui, J. Hu, F. Chu, Y. Zheng, J. Liu, C. Li, *ACS Nano* **2020**, *14*, 1866–1878.
- [31] J. Meng, C. Li, *Energy Storage Mater.* **2021**, *37*, 466–475.
- [32] M. Huang, Z. Yao, Q. Wu, Y. Zheng, J. Liu, C. Li, *ACS Appl. Mater. Interfaces* **2020**, *12*, 46132–46145.
- [33] K. Yan, Z. Lu, H.-W. Lee, F. Xiong, P.-C. Hsu, Y. Li, J. Zhao, S. Chu, Y. Cui, *Nat. Energy* **2016**, *1*, 16010.
- [34] A. Varzi, K. Thanner, R. Scipioni, D. Di Lecce, J. Hassoun, S. Dorfler, H. Altheus, S. Kaskel, C. Prehal, S. A. Freunberger, *J. Power Sources* **2020**, *480*, 228803.
- [35] D. Zhang, A. Dai, B. Fan, Y. Li, K. Shen, T. Xiao, G. Hou, H. Cao, *ACS Appl. Mater. Interfaces* **2020**, *12*, 31542–31551.
- [36] H. Mao, W. Yu, Z. Cai, G. Liu, L. Liu, R. Wen, Y. Su, H. Kou, K. Xi, B. Li, H. Zhao, X. Da, H. Wu, W. Yan, S. Ding, *Angew. Chem. Int. Ed.* **2021**, *60*, 19306–19313.
- [37] S. Huang, W. Zhang, H. Ming, G. Cao, L. Fan, H. Zhang, *Nano Lett.* **2019**, *19*, 1832–1837.
- [38] S. Zhang, G. Yang, Z. Liu, S. Weng, X. Li, X. Wang, Y. Gao, Z. Wang, L. Chen, *ACS Energy Lett.* **2021**, *6*, 4118–4126.
- [39] Z. Zhang, Y. Jin, Y. Zhao, J. Xu, B. Sun, K. Liu, H. Lu, N. Lv, Z. Dang, I. H. Wu, *Nano Res.* **2021**, *14*, 3999–4005.
- [40] C. Yang, Y. Yao, S. He, H. Xie, E. Hitz, L. Hu, *Adv. Mater.* **2017**, *29*, 1702714.
- [41] R. Zhang, X.-R. Chen, X. Chen, X.-B. Cheng, X.-Q. Zhang, C. Yan, Q. Zhang, *Angew. Chem.* **2017**, *129*, 7872–7876; *Angew. Chem. Int. Ed.* **2017**, *56*, 7764–7768.
- [42] L. Liu, Y.-X. Yin, J.-Y. Li, S.-H. Wang, Y.-G. Guo, L.-J. Wan, *Adv. Mater.* **2018**, *30*, 1706216.
- [43] C. Jin, O. Sheng, J. Luo, H. Yuan, C. Fang, W. Zhang, H. Huang, Y. Gan, Y. Xia, C. Liang, J. Zhang, X. Tao, *Nano Energy* **2017**, *37*, 177–186.
- [44] S. Wu, Z. Zhang, M. Lan, S. Yang, J. Cheng, J. Cai, J. Shen, Y. Zhu, K. Zhang, W. Zhang, *Adv. Mater.* **2018**, *30*, 1705830.
- [45] M. Zhu, B. Li, S. Li, Z. Du, Y. Gong, S. Yang, *Adv. Energy Mater.* **2018**, *8*, 1703505.
- [46] A. Pei, G. Zheng, F. Shi, Y. Li, Y. Cui, *Nano Lett.* **2017**, *17*, 1132–1139.
- [47] A. D. Pelton, *J. Phase Equilib.* **1991**, *12*, 42–45.
- [48] A. Varzi, L. Mattarozzi, S. Cattarin, P. Guerriero, S. Passerini, *Adv. Energy Mater.* **2017**, *8*, 1701706.

Manuscript received: August 21, 2022

Revised manuscript received: October 17, 2022

Accepted manuscript online: October 19, 2022

Version of record online: November 27, 2022